Simulation of the net snow accumulation along the Wilkes Land transect, Antarctica, with a regional climate model

Hubert Gallée, Vincent Peyaud, Ian Goodwin

Simulation of the net snow accumulation along the Wilkes Land transect, Antarctica, with a regional climate model

Hubert GALLÉE,[1] Vincent PEYAUD, Ian GOODWIN[2]

[1]*Laboratoire de Glaciologie et Géophysique de l'Environnement (CNRS–UJF), 54 rue Molière, BP 96, 38402 Saint-Martin-d'Hères Cedex, France*
E-mail: gallee@lgge.obs.ujf-grenoble.fr
[2]*Environmental Geoscience Group, School of Environmental and Life Sciences, University of Newcastle, Callaghan, New South Wales 2308, Australia*

ABSTRACT. Regional climate modelling in conjunction with accumulation measurements collected on Antarctic traverses of the International Trans-Antarctic Scientific Expedition (ITASE) is presented as a tool for extending the spatial coverage of field measurements. The modelling of part of East Antarctica spanned the 7 year epoch 1980–86 where data covering the same period are available. The agreement between simulation and observation is improved when a parameterization of the snow surface redistribution processes, such as wind erosion, is included in the regional climate model. The modelled spatial distribution of the net snow mass transported in the boundary layer over coastal East Antarctica indicates that this mass is a significant component of the surface mass balance.

1. INTRODUCTION

The contribution of all components of the Antarctic ice-sheet mass-balance variability to present and predicted sea level is poorly known. One such component is the surface mass balance (SMB) which is equivalent to precipitation plus snow redistribution by the wind minus sublimation, evaporation and melt. It is generally largest in the coastal regions of the Antarctic ice sheet and also experiences the greatest spatial and temporal variability. The SMB of coastal Antarctic regions is sensitive to circum-Antarctic atmosphere–ocean fluctuations and their effect on cyclone frequency and tracks. The temporal SMB signal is an important parameter for the detection of long-term climate change. Consequently, measurements of SMB and interpretation of SMB history are a key goal of the International Trans-Antarctic Scientific Expedition (ITASE). SMB data are obtained either by snow accumulation rate measurements on networks of snow stakes, or from interpretation of annual snow layer increments in snow pits or in firn and ice cores. Such data allow the validation of climate models and SMB models of the Antarctic ice sheet. Reciprocally, it is expected that the regional modelling will strengthen our understanding of SMB. This could provide guidance on intrinsic uncertainty in glaciological sampling that may be of relevance to ice-core interpretation. Indeed small-scale spatial variability in net observed SMB may preclude the determination of 'true' precipitation or SMB in large sectors of the Antarctic (Frezzotti and others, 2004). Finally, the regional modelling of SMB can provide useful data for planning optimal routes for proposed ITASE traverses.

Modelling studies of the Antarctic ice-sheet SMB have been conducted with global climate models (GCMs; for a review see Genthon and Krinner, 2001), and limited-area models (LAMs) used as regional climate models (RCMs, initialized once and nudged on the sides for the rest of the time; e.g. Van Lipzig and others, 2002a, b) or as regional numerical weather prediction models (RNWPs, initialized every few days; Guo and others, 2003). A process that has never been coupled to atmospheric dynamics at the climatic scale is snow transport by wind, although blowing-snow models are forced offline by meteorological fields to estimate the impact of snow redistribution by wind on the Antarctic SMB (Déry and Yau, 2002; Bromwich and others, 2004). Indeed it is suspected that such a process significantly impacts the SMB, at least in the coastal regions (Bromwich, 1988). The objectives of this paper are (i) to compare directly the outputs of a fine-resolution RCM with snow-stake measurements, and (ii) to examine the sensitivity of the simulated Antarctic ice-sheet SMB to snow redistribution by wind in the Wilkes Land region. The study uses the regional climate model MAR (Modèle Atmosphérique Régional) forced by large-scale meteorological fields from the European re-analyses ERA-15 (Gibson and others, 1997). This allows us to take into account 'realistic' large-scale meteorological fields in the simulation together with a representation of the boundary layer adapted to the polar regions in MAR, and to improve the simulation of the Antarctic surface conditions. MAR has already been validated over Antarctica for long-term simulations (Naithani and others, 2002).

2. SNOW ACCUMULATION FIELD MEASUREMENTS

We have applied MAR to the study of snow accumulation (precipitation plus snowdrift deposition minus erosion, evaporation and sublimation) across 1500 km of coastal Queen Mary Land and Wilkes Land. From 1980 to 1986, glaciologists from the Australian National Antarctic Research Expeditions (ANARE) measured snow accumulation across this region on snow stakes every 2 km, in snow pits and in shallow firn cores (Goodwin, 1995). The region experiences annual snow accumulation, even after significant precipitation losses through erosion of the snow surface by strong surface winds. Goodwin (1990) reported the relationship between the spatial snow accumulation pattern, mesoscale topography and the surface wind field, and Goodwin (1991) reported the temporal variability of snow accumulation over the period 1930–85. The spatial variability over 20 km windows was 14–34% of the mean values,

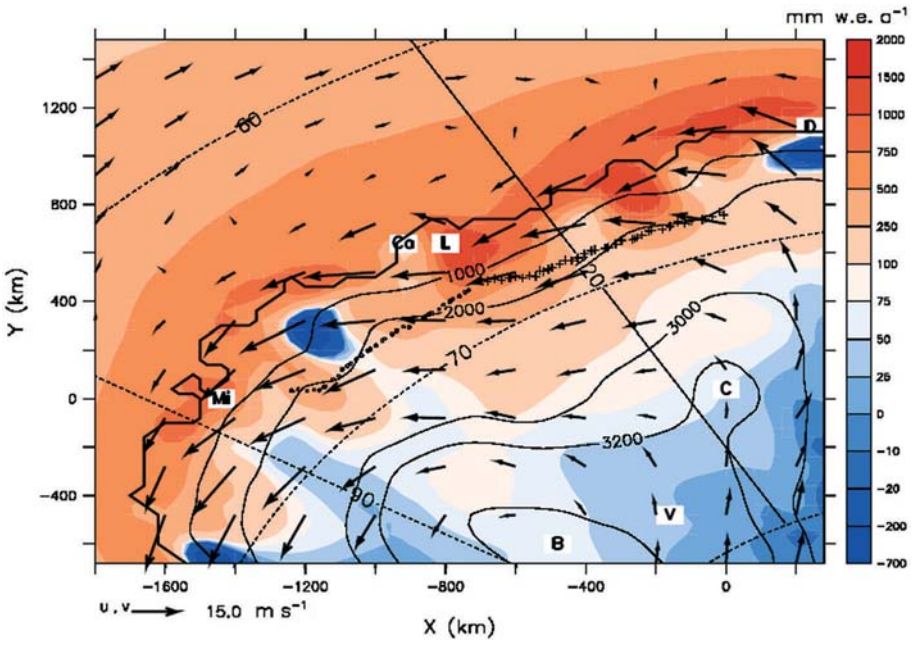

Fig. 1. The SMB and the wind vector 10 m above the surface simulated by MAR and averaged from 15 November 1980 until 15 November 1986. The western and eastern Australian traverses are indicated respectively by circles and crosses. Mi: Mirny; Ca: Casey; L: Law Dome; D: Dumont d'Urville; C: Dome C; V: Vostok; B: Ridge B.

whilst the interannual variability measured in the firn cores was estimated to be 20–30% of the 50 year mean values. The snow accumulation values used to validate the MAR were 1 and 3 year average values for each 20 km window. These data allowed a comprehensive comparison with the MAR output, and enabled the assessment of snow precipitation loss caused by surface wind erosion and redistribution and its impact on the SMB estimates.

3. MODEL DESCRIPTION

MAR has been developed for polar regions. A short description is given here, emphasizing recent modifications made for Antarctic climate simulations.

The dry version of the atmospheric model is fully described in Gallée and Schayes (1994). MAR is a hydrostatic primitive-equation model in which the vertical coordinate is the normalized pressure. No approximation is made in the mass-conservation equation, i.e. the compressible form is retained.

The representation of the hydrological cycle includes a cloud microphysical model, with conservation equations for cloud droplet, raindrop, cloud ice crystal and snowflake concentrations (Gallée, 1995). The description of the cloud microphysical processes is based on the Kessler (1969) parameterization. Ice microphysical processes are included based on the work of Lin and others (1983). The Fletcher (1962) equation for ice nuclei concentration is replaced with the more realistic parameterization of Meyers and others (1992). A prognostic equation for the ice crystal number is added, according to Levkov and others (1992), allowing explicit computation of the sedimentation of ice cloud particles.

Detailed solar and infrared radiation schemes are used in MAR. The solar radiation scheme is from Fouquart and Bonnel (1980). The longwave radiation scheme follows a wideband formulation of the radiative transfer equation (Morcrette, 1984) and was designed for use in GCMs. Cloud properties are taken into account in the solar and infrared radiation scheme by computing the liquid-water path in each model layer from the concentration of cloud droplets and ice crystals.

The atmospheric part of MAR is coupled to the soil–vegetation–atmosphere transfer (SVAT) scheme SISVAT (De Ridder and Gallée, 1998). SISVAT (soil–ice–snow–vegetation–atmosphere transfer) is a vertical one-dimensional model. The surface scheme includes soil–vegetation (De Ridder and Schayes, 1997), snow (Gallée and others, 2001) and an ice module (Lefebre and others, 2003). The snow model is a multi-layer model including prognostic equations for temperature, mass, water content and snow properties (dendricity, sphericity and size). The evolution of the snowpack properties is parameterized according to Brun and others (1992).

The coupling of SISVAT with the atmosphere is performed through the exchange of radiative (solar, infrared) fluxes and turbulent fluxes of momentum, heat (sensible, latent) and blown-snow particles. The bulk aerodynamic formulae used to describe the turbulent fluxes are modified to take into account the increase in vertical stability of the surface boundary layer due to snow erosion (Bintanja, 1998). In particular, the Monin–Obukhov length includes the contribution from the turbulent fluxes of blown-snow particles. Snow erosion by wind occurs for friction velocities larger than a threshold friction velocity which is parameterized as a function of the snow properties, according to Guyomarc'h and Mérindol (1998). The surface boundary condition for snow erosion is the snow particle concentration in the saltation layer, which is parameterized according to Pomeroy (1989). The blown-snow turbulent flux is included as a source term in the prognostic equation for snowflakes. Blown-snow particles may consequently sublimate and precipitate. The sedimentation velocity of snowflakes has not been modified, although a smaller sedimentation

Table 1. Simulated (sim) and observed (obs) wind speed V ($m\,s^{-1}$) and direction D (°) at Dumont d'Urville, Casey, Mirny and Vostok identified respectively by the labels D, Ca, Mi and V in Figure 1

	sim		obs	
	V	D	V	D
DdU	21.9	137	18.2	144
Casey	14.4	87	12.2	89.8
Mirny	16.1	100	21.7	–
Vostok	5.6	238	10.3	298

velocity of blown-snow particles is needed for calibrating simple blowing-snow models (Mann and others, 2000). Instead, the ratio of the turbulent diffusion coefficient for snowflakes to that of momentum is set to 3, as in Bintanja (2000). More details about the snow and the blowing-snow modules may be found in Gallée and others (2001). Finally, the roughness length for momentum and blown-snow particles is 0.1 mm. The roughness length for scalars is parameterized according to Andreas (1987).

4. MODEL SIMULATIONS

MAR is driven by large-scale meteorological fields from ERA-15. Note that some authors have pointed out an elevation problem with ERA-15 over Vostok which affects the moisture flux convergence over West Antarctica (e.g. Bromwich and others, 2000). The integration domain covers the part of Antarctica containing the Amery Ice Shelf, Wilkes Land, Victoria Land, the Ross Sea and the Ross Ice Shelf. South Pole is located in the domain, near the lateral boundary passing over the continent. The horizontal resolution is 40 km and the model topography is obtained by averaging the Antarctic digital elevation model (DEM) of Liu and others (2001) over the MAR grid. Here, we only consider the part of the domain including Ridge B, Vostok, Dome C and Wilkes Land (see Fig. 1). There are 33 levels in the vertical, with the finest resolution in the low troposphere. The five lowest levels are set at 10, 20, 40, 80 and 160 m above the ground.

The standard simulation is conducted for the years 1980–86. The snowpack is initialized with a density of 300 $kg\,m^{-3}$ and small rounded grains (sphericity = 1, size = 0.3 mm). The initial surface temperature is taken from ERA-15. All initial values of the snowpack variables are constant along the vertical. A sensitivity simulation is done by switching off the blowing-snow parameterization, for the same period. The output of the standard simulation on 1 July 1980 at 0000 UTC is used to initialize the sensitivity experiment.

Figure 1 shows the simulated SMB and the wind vector 10 m above the surface, averaged over the period between 15 November 1980 and 15 November 1986. A comparison between the simulated and observed wind speed and direction at four sites is shown in Table 1. The simulated wind direction agrees with the observations in the coastal zone, but the wind speed is overestimated at Dumont d'Urville, downwind of an ablation area, and at Casey, downwind of Law Dome. These points are discussed later. Stronger winds are simulated in topographic confluence zones, near the coast. The strongest winds are simulated over the ablation zones, where snow erosion by wind is larger than snow deposition and precipitation. The location of the ablation zones is generally well simulated by the model, although their extent and the erosion intensity there seem to be overestimated. The ablation zone centred around 70° S, 70° E ($x = -1450$ km, $y = -650$ km in Fig. 1) corresponds to that observed by Vaughan and others (1999) east of the Amery Ice Shelf. Other coastal ablation zones are simulated east of Mirny and south of Dumont d'Urville. The latter was observed by M. Pourchet (personal communication, 2003). These ablation zones, except the zone simulated on the eastern side of the Amery Ice Shelf, were also simulated by Gallée and others (2001). A large zone of weak ablation is simulated over the Antarctic Plateau, between the Ross Sea coast and a line from Dome C to Vostok. Frezzotti and others (2002) identified this as an area of megadune formation, where the SMB is negative or nil.

Table 2. Model performances. Mean ($mm\,w.e.\,a^{-1}$), rmse ($mm\,w.e.\,a^{-1}$) and efficiency index along the traverses. Dates are traverse periods. The distances refer to the line of stakes in Figure 1, starting from the westernmost stake. The western traverse (W36) is analyzed only between 120 and 720 km (see text)

		Eastern transect (720–1480 km)		Western transect (120–720 km)	
		E01 1980–81	E12 1981–82	E25 1982–85	W36 1983–86
Observation	Mean	440	324	300	329
Blowing snow *on*	Mean	459	441	308	285
	rmse	130	182	107	130
	Efficiency	0.376	0.122	0.113	0.284
Blowing snow *off*	Mean	469	483	409	388
	rmse	78	170	121	105
	Efficiency	0.189	0.045	–3.863	–1.189

Katabatic winds are generally strong and accelerating over the ablation zones, increasing erosion there. Continuing erosion where the SMB is already negative is simulated by MAR, resulting in an excessively negative SMB. This is not realistic and is probably due to the crude initialization of the snowpack properties. Note that small rounded grains may still be eroded under relatively strong wind conditions (see Gallée and others, 2001). Furthermore the formation of wind crusts precluding a subsequent erosion of snow is not represented in the model. This process is very efficient when the concentration of blown-snow particles is small. It occurs when the kinetic energy of falling blown-snow particles dissipates, causing partial melt and subsequent hardening of the snow surface (Goodwin, 1990). These two shortcomings have a much smaller impact in regions of high SMB such as in Wilkes Land. Overestimation of snow erosion by wind over the ablation zones may be responsible for overestimation of the wind speed downwind of these areas (see Fig. 1).

The model outputs were compared with snow-stake measurements made along the Australian traverses. The location of the stakes is indicated in Figure 1. The distances mentioned in the following refer to the line of stakes in Figure 1, starting from the westernmost stake. The snow-stake measurements and the MAR outputs are summarized in Table 2.

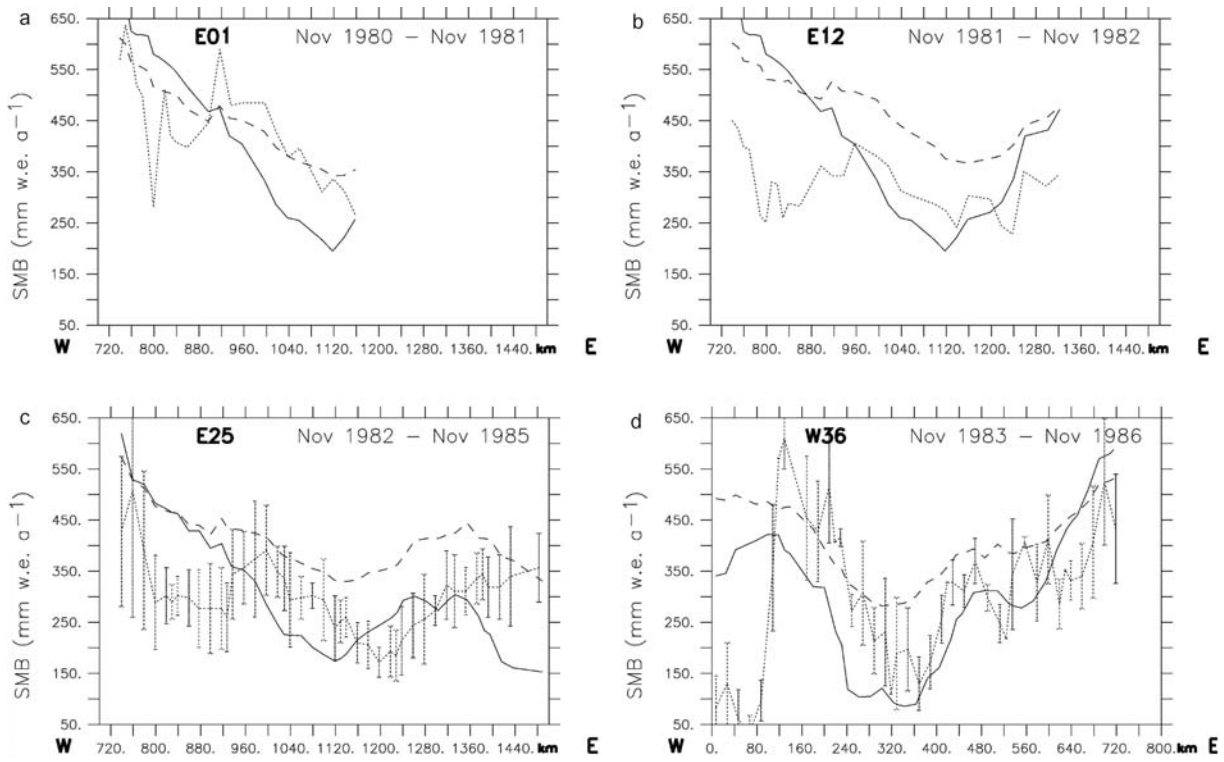

Fig. 2. Comparison between the MAR SMB simulation with and without snow redistribution by wind (solid and dashed lines respectively) and the snow-stake measurements (dotted line) made during the Australian traverses. The distances refer to the line of stakes in Figure 1, starting from the westernmost stake. (a) Eastern transect, traverse E01, 1980–81; (b) eastern transect, traverse E12, 1981–82; (c) eastern transect, traverse E25, 1982–85; and (d) western transect, traverse W36, 1983–86. The standard deviation of the measurements $\sqrt{\left[\Sigma(\mathrm{SMB}_{\mathrm{obs},i,j} - \overline{\mathrm{SMB}_{\mathrm{obs},i}})^2\right]/N}$ over each 20 km window i is also included for traverses E25 and W36 (vertical bars).

The spatial error of the model is measured in Table 2 for each traverse by the root-mean-square error

$$\mathrm{rmse} = \sqrt{\frac{\Sigma(\mathrm{SMB}_{\mathrm{sim},i} - \mathrm{SMB}_{\mathrm{obs},i})^2}{N}}, \quad (1)$$

where N is the number of 20 km windows used, and the efficiency index (Nash and Sutcliffe, 1970)

$$E = 1 - \frac{\Sigma(\mathrm{SMB}_{\mathrm{sim},i} - \mathrm{SMB}_{\mathrm{obs},i})^2}{\Sigma(\mathrm{SMB}_{\mathrm{sim},i} - \overline{\mathrm{SMB}_{\mathrm{sim}}})^2}. \quad (2)$$

An efficiency index close to 1 means that comparing the simulated $\mathrm{SMB}_{\mathrm{sim},i}$ with their corresponding observations $SMB_{\mathrm{obs},i}$ for each 20 km window i provides a lower rmse than that obtained when comparing the $\mathrm{SMB}_{\mathrm{sim},i}$ with their traverse average $\overline{\mathrm{SMB}_{\mathrm{sim}}}$. A negative efficiency index means that the rmse is larger than the standard deviation of the measurements, suggesting that a detailed model providing $\mathrm{SMB}_{\mathrm{sim},i}$ does not improve the results when compared to a simpler model providing an estimation of $\overline{\mathrm{SMB}_{\mathrm{sim}}}$ only.

Note that the first 125 km (situated on the western transect between 0 and 125 km; see Fig. 2d) have not been included in the Table 2 comparison because of the large differences (until roughly 400 m) between the topography measurements and the DEM used in MAR in that area.

The spatial error for each traverse is now analyzed. Comparisons between the measurements and the different periods of the simulation are presented in Figure 2. Measurements allow the observed SMB along the eastern transect to be determined for three periods: November 1980–November 1981 (traverse E01, Fig. 2a), November 1981–November 1982 (traverse E12, Fig. 2b) and November 1982–November 1985 (traverse E25, Fig. 2c). One period, November 1983–November 1986 (Fig. 2d), is available for the western transect (traverse W36). As the horizontal grid size of the model (40 km) is larger than the distance between the stakes, the model outputs are linearly interpolated at the stake locations.

The agreement between the simulated and observed SMB is generally good, but some discrepancies are found. The model does not simulate well the SMB over the eastern traverses between 720 and 920 km (see horizontal axis of Figure 2a–c for identification of these distances). This problem is more marked for traverses E12 and E25, and accounts for a lower efficiency index for these two traverses than for traverse E01. The decrease in the accumulation rate is well simulated after 920 km. In fact the model does not simulate the SMB minimum in the first part of the eastern traverses, i.e. between 720 and 880 km. Rather, the simulated decrease in accumulation with increased elevation is in agreement with a SMB model of Wilkes Land. Goodwin (1990) assumed that the local minimum in the observed SMB is due to shading of the precipitation by Law Dome, identified by 'L' in Figure 1 and situated to the north of the stake set at 720 km. He pointed out that this influence is not taken into account in the above-mentioned SMB model. Law Dome is also not well represented in the model topography. It is included in the DEM used to force MAR, but its elevation (1390 m) is underestimated (as 985 m) because of the use of a relatively coarse resolution (40 km). It is possible that the actual elevation of Law Dome is sufficient to block significantly the precipitation generated in the

lower troposphere (see, e.g., Bromwich, 1988) and advected southward over the ice sheet, and that this is not captured by the model topography.

The comparison with the sensitivity experiment (blowing-snow parameterization switched off; Fig. 2a and b) provides a possible additional explanation. Snow redistribution by wind slightly amplifies the SMB southward of Law Dome, so it may be argued that the low-level wind is not well simulated there. This is significant, as Law Dome markedly influences extreme wind events (Murphy, 2003) and is not well represented in the model topography. A much finer-resolution simulation is needed to clarify this point.

The simulated SMB has a maximum at 1360 km, on the eastern part of the E25 traverse (see Fig. 2c), while the observed maximum is further east. As this discrepancy is also found when the blowing-snow parameterization is switched off, it cannot be explained by overestimation of snow erosion by wind. Goodwin (1990) reported that longitudinal snow-dune fields and anomalously high accumulation characterized this region. Possibly the model is simulating the wind field correctly but not the precipitation in that area.

The impact of snow redistribution by wind is assessed by including the results of the sensitivity experiment (blowing-snow parameterization switched off) in Figure 2 and Table 2. The simulated SMB averaged over each traverse, $\overline{\mathrm{SMB}_{\mathrm{sim}}}$, is in better agreement with that observed, $\overline{\mathrm{SMB}_{\mathrm{obs}}}$, when the parameterization of blowing snow is included in the model. In contrast, the rmse is higher, except for traverse E25, but the efficiency index is better (positive and closer to 1) for all traverses. This may indicate that the improvement in performance due to better simulation of the averaged SMB is more effective than the decrease due to a larger rmse. Note, however, that a large rmse is not surprising since the relatively important standard deviation of the measurements suggests that their accuracy may be as poor as that of the model (see Fig. 2).

The SMB is systematically overestimated in 1981–82 when the blowing-snow parameterization is switched off (traverse E12; see Fig. 2b). In fact the amplitude of the simulated SMB extrema is more pronounced when that process is taken into account. The model still overestimates the SMB over traverse E25 (eastern transect, 1982–85) when the blowing-snow parameterization is switched off. The SMB minimum at 1120 km is not well marked in this case. In contrast, the well-simulated SMB between 1120 and 1360 km in the blowing-snow case may be correlated to a wind-speed maximum simulated in that area.

The results of the sensitivity experiment have also been compared with those of the standard over the western traverse (1983–86; Fig. 2d). Better agreement is found when the snow redistribution by wind is taken into account in the model, in particular when considering the SMB minimum, which is more pronounced. The area of the SMB minimum corresponds to a region of enhanced katabatic winds. Nevertheless, snow erosion by wind is slightly overestimated in this area.

The divergence of the fluxes of horizontal snow particles and water vapour in the katabatic layer has also been computed (not shown here). This gives the corresponding snow erosion on the surface and the snow sublimation (from the surface and from blown-snow particles). Snow erosion by wind represents about 50–100 mm w.e. a^{-1} in the traverse area and becomes more important for lower surface elevations, in agreement with the traverse profiles (Fig. 2). Finally, about one-third of these blown-snow particles sublimate.

The temporal variability of the simulated SMB was also compared to that of the measurements made over the eastern transect. This evaluation of the model is more qualitative since we have measurements of the SMB over three periods only. Nevertheless it is found in Table 2 that the model simulates an increase of the mean SMB ($\overline{\mathrm{SMB}_{\mathrm{sim}}}$) from 1980–81 to 1982–85, as in the observations. This trend is not simulated when the blowing-snow parameterization is switched off. This result needs to be confirmed, but it highlights the influence of snow redistribution on the temporal variability of accumulation, as already pointed out by Frezzotti and others (2004).

The model simulates snow accumulation over the Antarctic Plateau relatively well. It is found that the simulated snow net accumulation at Vostok for the period 1981–86 is 28 mm w.e. a^{-1}, in good agreement with observations (24 mm w.e. a^{-1}; Barkov and Lipenkov, 1996). The abrupt increase in accumulation to the northeast of Dome C observed by Siegert (2003) is also well simulated. A more detailed comparison of the snow accumulation with the observations over the plateau will be the subject of another paper.

5. CONCLUSIONS

The regional climate model MAR is applied for a long-term simulation of the Antarctic SMB. The impact of snow redistribution by wind is taken into account.

This is the first time that a long simulation of the Antarctic climate (several years) has been performed with a RCM (i.e. a LAM initialized once and nudged on the sides for the rest of the time) using such a fine resolution and having parameterizations substantially different from those of GCMs (i.e. atmospheric turbulence including the influence of snow erosion by wind, and prognostic equation describing the blown-snow particles concentration). In addition, detailed cloud microphysics with prognostic equations for cloud ice and droplets, snow and rain are included, as in a few other RCMs and RNWPs. The model-simulated snow accumulations in the coastal zone and over the Antarctic Plateau are generally realistic, in contrast with previous studies (Genthon and Krinner, 2001), in which the SMB was overestimated in the coastal region and underestimated over the plateau. This improvement is probably due to the use of the above-mentioned improved parameterizations of the model physics. Nevertheless the erosion of snow by the wind is overestimated in the ablation areas, probably because of a crude initialization of the snowpack properties.

This is also the first time that snow accumulation rate measurements and model outputs have been directly compared for the same time periods and for a fine horizontal resolution. The model is found to simulate well the spatial and temporal variability of the SMB in a high-accumulation region. This will allow the use of model outputs as a preliminary estimation of new snow accumulation measurements and the subsequent optimization of routes for new traverses.

ACKNOWLEDGEMENTS

The supercomputing center IDRIS (Institut de Développement et des Ressources en Informatique Scientifique) of the

Centre National de la Recherche Scientifique, France, is acknowledged for providing support to this project. The Action Concertée Incitative Risques Naturels et Changements Climatique C3 of the Fond National de la Science, the Programme National d'Etudes de la Dynamique du Climat (PNEDC) and the Programme d'études de l'ATmosphère et de l'Océan à Multiéchelles (PATOM) are acknowledged for financial support of the project.

REFERENCES

Andreas, E.L. 1987. A theory for the scalar roughness and the scalar transfer coefficients over snow and sea ice. *Bound.-Lay. Meteorol.,* **38**(1–2), 159–184.

Barkov, N.I. and V.Y. Lipenkov. 1996. Nakopleniye snega v rayone stantsii Vostok, Antarktida, v 1970–1992 gg. *Mater. Glyatsiol. Issled.,* **80**, 87–88.

Bintanja, R. 1998. The interaction between drifting snow and atmospheric turbulence. *Ann. Glaciol.,* **26**, 167–173.

Bintanja, R. 2000. Snowdrift suspension and atmospheric turbulence. II. Results of model experiments. *Bound.-Lay. Meteorol.,* **95**, 369–395.

Bromwich, D.H. 1988. Snowfall in high southern latitudes. *Rev. Geophys.,* **26**(1), 149–168.

Bromwich, D.H., A.N. Rogers, P. Kållberg, R.I. Cullather, J.W.C. White and K.J. Kreutz. 2000. ECMWF analyses and reanalyses depiction of ENSO signal in Antarctic precipitation. *J. Climate,* **13**(8), 1406–1420.

Bromwich, D.H., Z. Guo, L. Bai and Q. Chen. 2004. Modelled Antarctic precipitation. Part I: spatial and temporal variability. *J. Climate,* **17**(3), 427–447.

Brun, E., P. David, M. Sudul and G. Brunot. 1992. A numerical model to simulate snow-cover stratigraphy for operational avalanche forecasting. *J. Glaciol.,* **38**(128), 13–22.

De Ridder, K. and H. Gallée. 1998. Land surface-induced regional climate change in Southern Israel. *J. Appl. Meteorol.,* **37**(11), 1470–1485.

De Ridder, K. and G. Schayes. 1997. The IAGL land surface model. *J. Appl. Meteorol.,* **36**, 167–182.

Déry, S.J. and M.K. Yau. 2002. Large-scale mass balance effects of blowing snow and surface sublimation. *J. Geophys. Res.,* **107**(D23), 4679. (10.1029/2001JD001251.)

Fletcher, N.H. 1962. *The physics of rainclouds*. Cambridge, Cambridge University Press.

Fouquart, Y. and B. Bonnel. 1980. Computations of solar heating of the Earth's atmosphere: a new parameterization. *Beitr. Phys. Atmosph.,* **53**(1), 35–62.

Frezzotti, M., S. Gandolfi, F. La Marca and S. Urbini. 2002. Snow dunes and glazed surfaces in Antarctica: new field and remote-sensing data. *Ann. Glaciol.,* **34**, 81–88.

Frezzotti, M. *and 12 others*. 2004. New estimations of precipitation and surface sublimation in East Antarctica from snow accumulation measurements. *Climate Dyn.,* **23**(7–8), 803–813.

Gallée, H. 1995. Simulation of the mesocyclonic acitivity in the Ross Sea, Antarctica. *Mon. Weather Rev.,* **123**(7), 2051–2069.

Gallée, H. and G. Schayes. 1994. Development of a three-dimensional meso-γ primitive equations model: katabatic wind simulation in the area of Terra Nova Bay, Antarctica. *Mon. Weather Rev.,* **122**(4), 671–685.

Gallée, H., G. Guyomarc'h and E. Brun. 2001. Impact of snowdrift on the Antarctic ice sheet surface mass balance: possible sensitivity to snow-surface properties. *Bound.-Lay. Meteorol.,* **99**(1), 1–19.

Genthon, C. and G. Krinner. 2001. The Antarctic surface mass balance and systematic biases in GCMs. *J. Geophys. Res.,* **106**(D18), 20,653–20,664.

Gibson, R., P. Kållberg, S. Uppala, A. Hernandez, A. Nomura and E. Serrano. 1997. *ERA description*. Reading, European Centre for Medium-Range Weather Forecasts. (ECMWF Re-Analysis Project Report Series 1.)

Goodwin, I.D. 1990. Snow accumulation and surface topography in the katabatic zone of eastern Wilkes Land, Antarctica. *Antarct. Sci.,* **2**(3), 235–242.

Goodwin, I.D. 1991. Snow-accumulation variability from seasonal surface observations and firn-core stratigraphy, eastern Wilkes Land, Antarctica. *J. Glaciol.,* **37**(127), 383–387.

Goodwin, I.D. 1995. On the Antarctic contribution to Holocene sea-level. (PhD thesis, University of Tasmania.)

Guo, Z., D.H. Bromwich and J.J. Cassano. 2003. Evaluation of Polar MM5 simulations of Antarctic atmospheric circulation. *Mon. Weather Rev.,* **131**, 384–411.

Guyomarc'h, G. and L. Mérindol. 1998. Validation of an application for forecasting blowing snow. *Ann. Glaciol.,* **26**, 138–143.

Kessler, E. 1969. On the distribution and continuity of water substance in atmospheric circulation. *Meteorol. Monogr.* 32-84.

Lefebre, F., H. Gallée, J.P. Ypersele and W. Greuell. 2003. Modeling of snow and ice melt at ETH camp (West Greenland): a study of surface albedo. *J. Geophys. Res.,* **108**(D8), 4231. (10.1029/2001JD001160.)

Levkov, L., B. Rockel, H. Kapitza and E. Raschke. 1992. 3D mesoscale numerical studies of cirrus and stratus clouds by their time and space evolution. *Beitr. Phys. Atmosph.,* **65**, 35–57.

Lin, Y.-L., R.D. Farley and H.D. Orville. 1983. Bulk parameterization of the snow field in a cloud model. *J. Appl. Meteorol.,* **22**(6), 1065–1092.

Liu, H., K.C. Jezek, B. Li and Z. Zhao. 2001. *RADARSAT Antarctic Mapping Project digital elevation model. Version 2*. Boulder, CO, National Snow and Ice Data Center.

Mann, G.W., P.S. Anderson and S.D. Mobbs. 2000. Profile measurements of blowing snow at Halley, Antarctica. *J. Geophys. Res.,* **105**(D19), 24,491–24,508.

Meyers, M.P., P.J. Demott and W.R. Cotton. 1992. New primary ice-nucleation parameterizations in an explicit cloud model. *J. Appl. Meteorol.,* **31**(7), 708–721.

Morcrette, J.J. 1984. Sur la paramétrisation du rayonnement dans les modèles de la circulation générale atmosphérique. (PhD thesis, Université des Sciences et Techniques de Lille.)

Murphy, B.F. 2003. Prediction of severe synoptic events in coastal East Antarctica. *Mon. Weather Rev.,* **131**(2), 354–370.

Naithani, J., H. Gallée and G. Schayes. 2002. Marine air intrusion into the Adelie Land sector of East Antarctica: a study using the regional climate model (MAR). *J. Geophys. Res.,* **107**(D11), 4124. (10.1029/2000JD000274.)

Nash, J.E. and J.V. Sutcliffe. 1970. River flow forecasting through conceptual models. Part 1. A discussion of principles. *J. Hydrol.,* **10**(3), 282–290.

Pomeroy, J.W. 1989. A process-based model of snow drifting. *Ann. Glaciol.,* **13**, 237–240.

Siegert, M.J. 2003. Glacial–interglacial variations in central East Antarctic ice accumulation rates. *Quat. Sci. Rev.,* **22**(5–7), 741–750.

Van Lipzig, N.P.M., E. van Meijgaard and J. Oerlemans. 2002a. The spatial and temporal variability of the surface mass balance in Antarctica: results from a regional climate model. *Int. J. Climatol.,* **22**, 1197–1217.

Van Lipzig, N.P.M., E. van Meijgaard and J. Oerlemans. 2002b. Temperature sensitivity of the Antarctic surface mass balance in a regional climate model. *J. Climate,* **15**(19), 2758–2774.

Vaughan, D.G., J.L. Bamber, M.B. Giovinetto, J. Russell and A.P.R. Cooper. 1999. Reassessment of net surface mass balance in Antarctica. *J. Climate,* **12**(4), 933–946.